




# Native Point Defects in Monolayer Hexagonal Boron Phosphide from First Principles

ZIJIANG LUO,<sup>1</sup> YUANDONG MA,<sup>1</sup> XIUZHANG YANG,<sup>1</sup> BING LV,<sup>2</sup>  
ZHIBIN GAO,<sup>3</sup> ZHAO DING,<sup>4,5</sup> and XUEFEI LIU <sup>2,6</sup>

1.—School of Information, Guizhou University of Finance and Economics, Guiyang 550025, China. 2.—Key Laboratory of Low Dimensional Condensed Matter Physics of Higher Educational Institution of Guizhou Province, School of Physics and Electronic Science, Guizhou Normal University, Guiyang 550025, China. 3.—Department of Physics, National University of Singapore, Singapore 117551, Republic of Singapore. 4.—College of Big Data and Information Engineering, Guizhou University, Guiyang 550025, China. 5.—e-mail: zding@gzu.edu.cn. 6.—e-mail: 201307129@gznu.edu.cn

In this paper, we have investigated the electronic and magnetic properties of four types of native defects under neutral and charged states in a hexagonal boron phosphide (h-BP) monolayer, including boron vacancy ( $V_B$ ), phosphorus vacancy ( $V_P$ ), boron on the phosphorus site ( $B_P$ ) and phosphorus on the boron site ( $P_B$ ) within the framework of the density functional theory. For the four types of defects, various charge states were investigated, and only 0 and 1 + charge states for all defects are stable within the electronic chemical potential range (i.e. Fermi level range). It is found that  $B_P$  with the smallest defect formation energy is the most stable defect under both phosphorus-rich and -poor conditions in the whole range of electronic chemical potential.  $V_P$  and  $P_B$  are found to be shallow donors (i.e. 1 +/0) but could not be effectively introduced into the h-BP monolayer due to a rather high formation energy, while  $V_B$  and  $B_P$  are found to be holes trap centers. Especially,  $B_P$  with a low defect formation energy, will be produced easily and seriously affect the  $p$ -type doping efficiency and conductivity of h-BP. Additionally,  $V_B$  and  $V_P$  induce a nonzero magnetic moment while  $P_B$  and  $B_P$  show non-magnetic nature in the h-BP monolayer.

**Key words:** h-BP, vacancy, two-dimensional material, anti-site, native point charge defect, DFT computations

## INTRODUCTION

Boron phosphide (BP) has previously been proven to be stable in a cubic zinc-blende bulk structure at room temperature<sup>1,2</sup> and also was found to have promising mechanical, thermal, and electrical properties,<sup>3</sup> as well as  $n$ - and  $p$ -type doping ability.<sup>4</sup> Additionally, BP film is of interest for the development of a high-efficiency solid-state thermal neutron detector. Li et al. have reported that BP films can be grown on silicon carbide with vicinal steps and found that the films are epitaxial in the near-

interface region but deviate from epitaxial growth as the film develops.<sup>5</sup> These outstanding properties of bulk or film BP make it attractive for various electronic device applications. In addition, Feng et al. have produced micron-sized cubic BP particles with high purity and structural stability successfully.<sup>6</sup> Sugimoto and colleagues have synthesized BP nanocrystals (< 5 nm) and found the photocatalytic activity is size-dependent,<sup>7</sup> i.e. the quantum size effects can improve the photocatalytic activity. As mentioned above, it is found that the studied dimensions of BP is gradually scaling down.

Recently, owing to the superior thermal, mechanical and optoelectronic properties, an abundance of two-dimensional (2D) materials such as graphene,<sup>8,9</sup> phosphorene,<sup>10</sup> transition metal

(Received April 10, 2020; accepted July 24, 2020;  
published online August 9, 2020)

dichalcogenides,<sup>11–14</sup> graphitic carbon nitride,<sup>15,16</sup> borophene,<sup>17</sup> and III-N(BN, AlN, GaN, InN)<sup>18–21</sup> have been investigated theoretically or experimentally, and there have been many 2D materials successfully prepared as well as many 2D-based prototype devices.<sup>22,23</sup> Thus, single-layer (or few-layer) BP with a hexagonal structure has attracted increasing attention from theorists.<sup>24–30</sup> Çakır et al. have investigated the electronic and mechanical properties of single-layer hexagonal boron phosphide (h-BP), and they showed that h-BP is mechanically stable with a direct bandgap of 0.9 eV.<sup>31</sup> The phonon dispersion of h-BP shows no imaginary frequencies, which means that this monolayer structure is dynamically stable.<sup>31</sup> B-P bonds are not broken based on the Born–Oppenheimer Molecular Dynamics simulations at temperatures over 2000 K, showing strong thermal stability.<sup>32</sup> Shi et al. have reported that 2D h-BP can function as a highly stable and metal-free photocatalyst to produce hydrogen from water in the presence of sacrificial agents under visible light irradiation, even at extreme conditions such as strong acid and alkali.<sup>33</sup> Jiang et al. found that the alkali metal atoms show high diffusivities on the h-BP monolayer, showing the valuable potential application in metal-based batteries.<sup>34</sup> The electronic and optical properties of novel boron phosphide-based heterojunctions were also investigated,<sup>35–37</sup> as well as the high carrier mobility in the monolayer h-BP.<sup>38</sup> Graphene-like BP was also investigated theoretically.<sup>39</sup> In addition, in our previous work,<sup>19</sup> we have systematically calculated the mechanical properties of 25 kinds of III–V group 2D structures. We found that the III–V group binary compound consisting of smaller atoms with a larger Young’s modulus is more stable. For instance, h-BN, h-AlN, and h-GaN with Young’s moduli of 276 N/m, 113 N/m, and 106 N/m, respectively, have already been prepared successfully.<sup>40–44</sup> Thus, although the 2D h-BP has not been successfully synthesized currently, based on the rich synthesis experiences in other 2D materials, as well as a large number of theoretical evidence about the stability of single-layer h-BP, we believe h-BP, with a Young’s modulus of 139 N/m and a similar structure to other 2D III-Ns, will be synthesized in future.

As is known, it is inevitable to introduce native point defects, such as vacancy and anti-substitute defects, during the fabrication of h-BP, which seriously affects its optical and electronic properties.<sup>45,46</sup> In addition, the native point defects affect the *n*- or *p*-doping efficiency for semiconductor materials.<sup>47,48</sup> Thus, it is beneficial to explore the underlying physics about charged native point defects in the h-BP monolayer, to study how these defects affect the doping efficiency and to check whether they contribute to the *n*- or *p*-doping carriers in h-BP. However, a systematic study on

the charged native point defects in h-BP is still lacking. Ref. 24 investigated the anti-site and Stone–Wales defect in monolayer h-BP, but not in the charged case, thus they failed to explain the doping efficiency in monolayer h-BP.

In this work, by using advanced 2D charged defect calculation,<sup>49</sup> we mainly focus on the native point defect properties of 2D h-BP. Specifically, we have systematically investigated the formation energies, charge transition levels (CTLs) and other electronic properties of intrinsic defects in a monolayer h-BP by using first-principles methods based on density functional theory (DFT). B vacancy ( $V_B$ ), P vacancy ( $V_P$ ), anti-site B on P ( $B_P$ ) and anti-site P on B ( $P_B$ ) ranging from 3 – to 3 + charge states have been calculated. Usually, when the realistic charge state of certain defects cannot be determined, to consider a wider and relative reasonable charge range to guarantee the most stable charge state to be included is a common choice. Based on this consideration, the charge ranges in this paper were determined by the method in Ref. 50, where the authors implemented the charge-determined algorithm based on bond-valence theory in their PyCDT code.<sup>50</sup> The paper is organized as follows. In “[Computation Methods](#)”, the computation methods are described, “[Results and Discussion](#)” presents the results and discussions and a short summary is given in “[Conclusions](#)”.

## COMPUTATION METHODS

All results were calculated with the Vienna Ab initio Simulation Package (VASP) code.<sup>51</sup> During the calculations, generalized gradient approximation Perdew–Burke–Ernzerhof (GGA-PBE) functional<sup>52</sup> was used and spin-polarization was considered. The projector augmented wave (PAW) potential<sup>53</sup> files were used to construct the POT-CARs. To overcome the underestimate of the bandgap, a hybrid functional such as Heyd–Scuseria–Ernzerhof (HSE<sup>54</sup>) was used. The plane-wave cutoff was set to 400 eV and reciprocal space was sampled with a k-point mesh of  $23 \times 23 \times 1$  in the primitive cell for bandgap calculation. During the calculations, we redefined the lattice of hexagonal BP primitive into an orthogonal form with VASP-KIT code<sup>55</sup> and the minimum repeat unit includes four atoms (blue rectangles in Fig. 1). We have used a  $6 \times 6$  supercell (144 atoms) with a vacuum thickness of 45 Å to conduct the charged point defects calculations. In our previous paper,<sup>48</sup> we have found that a  $5 \times 5$  supercell (100 atoms) is large enough to meet the requirement of charged defect calculation under a reasonable post-correction method. Here, to obtain more reliable results, we chose a larger supercell, i.e. a  $6 \times 6$  supercell. All atoms were relaxed until the Hellman–Feynman force on individual atoms was less than 0.01 eV/Å

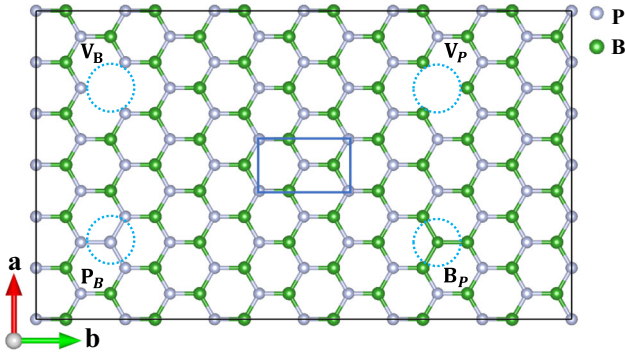


Fig. 1. The  $(6 \times 6)$  supercell (with 144 atoms), with the minimum repeat unit of h-BP highlighted by the blue rectangle. The sketch map of four intrinsic defects is marked by blue dotted circles (Color figure online).

and the total energy difference between two successive steps was lower than  $10^{-6}$  eV.

In the charged-defect calculations, to ensure the convergence of total energy during the self-consistent iteration process, a uniform background charge is added to the supercell.<sup>45</sup> The defect formation energy of a point defect  $x$  in charge state  $q$  in a finite supercell is given as below<sup>56</sup>:

$$E_{\text{finite}}^{\text{def}}[x^q] = E_{\text{def}}[x^q] - E_{\text{perfect}} - \sum n_i \mu_i + q(E_f + \epsilon_{\text{vbm}}^{\text{perfect}} - \Delta V_{0,p}) + E_{\text{correct}} \quad (1)$$

$E_{\text{def}}[x^q]$  is the total energy of a system containing a defect  $x$  in charge state  $q$ ,  $E_{\text{perfect}}$  represents the energy of the perfect supercell,  $n_i$  is the number of atoms of type  $i$  added (positive) or removed (negative) from the perfect system,  $\mu_i$  ( $i = B, P$ ) is the atom's chemical potential in its stable phase. For instance, under phosphorus-rich conditions,  $\mu_P = \mu_{P[\text{bulk}]}$  while under phosphorus-poor conditions,  $\mu_P = \mu_{BP[\text{bulk}]} - \mu_{B[\text{bulk}]}$ ,  $E_f$  is the Fermi level (or electron chemical potential) with respect to the valence band maximum (VBM),  $\epsilon_{\text{vbm}}^{\text{perfect}}$  of a perfect structure, ranging from VBM to bandgap ( $E_{\text{gap}}$ ), where  $E_f$  ranges from 0 to  $E_{\text{gap}}/2$ , the corresponding BP system is  $p$ -doped, while  $E_{\text{gap}}$  ranges from  $E_{\text{gap}}/2$  to  $E_{\text{gap}}$ , the corresponding BP system is  $n$ -doped.

$$\Delta V_{0,p} = V_0|_{\text{far}} - V_p \quad (2)$$

is a potential alignment term found by comparing the electrostatic potentials from a perfect supercell calculation and far from the defect in a neutral defect calculation,<sup>56</sup> which was on the order of  $\sim 0.05$  eV.  $E_{\text{correct}}$  is a correction term by Freysoldt and Neugebauer (FN) method,<sup>49</sup> which was proposed to calculate the formation energy of charged defects at surfaces, interfaces, or two-dimensional materials, and one does not need to resort to the finite-size extrapolation to obtain the isolated energy.

## RESULTS AND DISCUSSION

In this study, all structures with native defects under different charge states were fully optimized during the calculations. The bond lengths around the defects after relaxing were found to increase or decrease less than 0.1 Å, indicating our supercells are large enough.

### Density of States

We have considered four types of intrinsic defects in our current study, namely boron vacancy ( $V_B$ ), phosphorus vacancy ( $V_P$ ), boron on the phosphorus site ( $B_P$ ) and phosphorus on the boron site ( $P_B$ ). The density of states (DOS) is plotted in Fig. 2. The most stable charged states (MSCS) were found to be 0 and 1 + charge states (see next section); therefore, we will just discuss the DOS results on the two cases in the following sections.

The bandgap of pristine 2D h-BP under PBE and HSE level is 0.75 eV and 1.2 eV, respectively, which is much smaller than that of h-BN;<sup>48</sup> thus, the MSCS is different from that of h-BN. It can be found that for  $V_P$  (Fig. 2a) and  $P_B$  (Fig. 2d) under the neutral state, the Fermi levels are moved to conduction band minimum (CBM) while for  $V_B$  (Fig. 2b) and  $B_P$  (Fig. 2c) the position of Fermi level is almost fixed. Based on the DOS, it seems that  $V_B$  and  $B_P$  show a  $p$ -type semiconductor nature while  $V_P$  and  $P_B$  show an  $n$ -type nature. It can be concluded that these hole or electron carriers are derived from the dangling bonds when defects are introduced in h-BP, which was confirmed by the spin density distributions (not shown here for simplicity). Additionally, for the  $V_B$  system, three unoccupied states were found. Two of them are located at VBM + 0.4 eV and the other occupied state is located near the Fermi level close to VBM, resulting in a magnetic moment of 3  $\mu_B$ .

The results show that the magnetism of each defect system is relevant to the charge state. The underlying physics can be explained by electron configuration, as shown in Fig. 3. The electron configuration of phosphorus and boron atoms are  $3s^2 3p^3$  and  $2s^2 2p^1$ , when boron and phosphorus are bonded to form the h-BP layer structure, one electron from the s orbit in the boron atom is excited into the p orbit, thus reconfiguring the electrons as  $2s^1 2p^2$ , similarly, the electrons of the phosphorus atom are reconfigured as  $3s^1 3p^4$  and two electrons from the p orbit are paired. Consequently, an  $sp^2$  hybrid orbit is formed to maintain the h-BP stable and a planar structure. As all the electrons are paired, no magnetic moment was found in pristine h-BP. However, when a phosphorus atom is removed from the h-BP monolayer, the electron configuration of boron is recovered as  $2s^2 2p^1$ , the single electron in the p orbit induces intrinsic magnetism with a net magnetic moment of 1  $\mu_B$ , and  $V_P^{+1}$  is nonmagnetic due to the loss of the

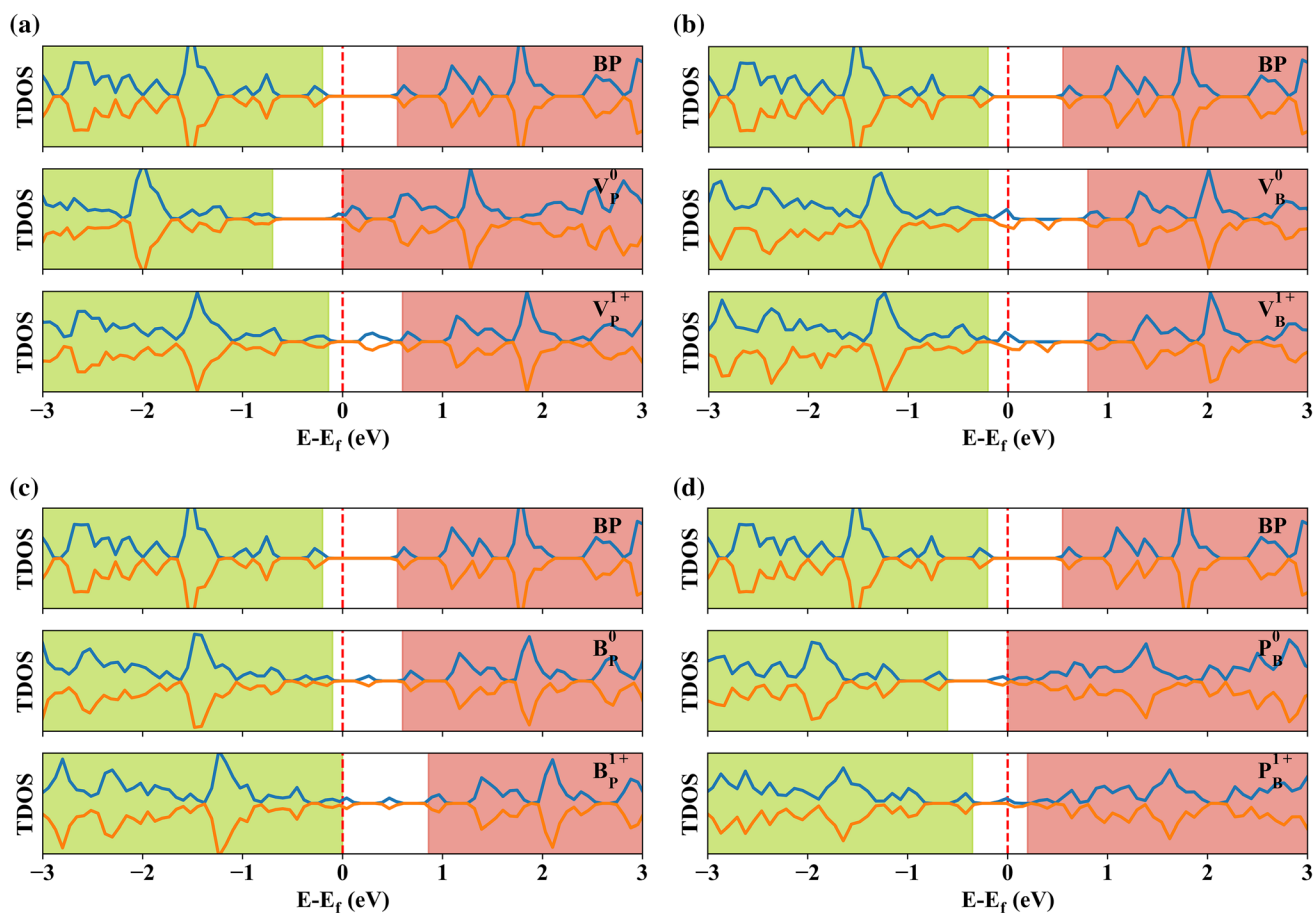


Fig. 2. The spin DOS of native point defects of 2D h-BP in different charge states. (a) For  $V_P$ , (b) for  $V_B$ , (c) for  $B_P$  and (d) for  $P_B$ , the Fermi level is aligned to 0 eV for all charge states.

single electron in the p orbit. A similar analysis about magnetic nature in other defect types can be done but is omitted for simplicity.

### Defect Formation Energy

It is important to predict the ionization energies for donors or acceptors by investigating the stability of the native point defects under different charge states. Based on formula (1), in this study, we calculated all the possible charge states (i.e. from 3 – to 3 +) for all types of defects, and the results show that only 0 and 1 + charge states are stable for all types of defects. Herein, the Fermi level was changed from 0 eV (VBM) to  $E_{gap}$ , thus different charge states lead to different slope curves and cross each other. The so-called MSCSs are defined as these line segments with different slopes (i.e. charge states) and are found with the smallest formation energy at certain Fermi levels, as shown in Fig. 4. All the defect formation energies were corrected with the FN method.<sup>49</sup> The result of defect formation energy of 1 + charge state is  $\sim 0.5$  eV higher than raw data without any correction. Note that adding or removing a charge  $q$  to the calculated structures does not mean the crystal is charged in a

realistic way, like that of an atom obtaining or losing an electron, which indeed comes from an external circumstance or goes to the vacuum zones. Taking  $q +$  as an example, it means there are  $q$  electrons removed from donor defect states in the bandgap and added to the host states of the h-BP materials, e.g. the CBM (at  $T = 0$  K). Similarly,  $q -$  means that  $q$  electrons are removed from the VBM and added to the acceptor states in the bandgap. The density derived electrostatic and chemical (DDEC) approach can be performed for analysis of interionic charge transfer and bond orders by the influence of vacancy.<sup>57–59</sup> However, in this paper we did not perform this kind of calculation for simplicity and highlight our main motivation of this study.

The accuracy of defect formation energies and CTLs are significantly impacted by the bandgap.<sup>45,46</sup> HSE overcomes the bandgap underestimation problem, but it is time-consuming, especially for a large supercell. It is noted that despite the bandgap narrowing by the semi-local GGA functional, the calculated formation energy is similar to that by HSE functional.<sup>44,48,60</sup> Thus, the derived defect transition level from PBE functional can be rescaled to the HSE level.<sup>44,48,60</sup> This method was used in this paper, and the PBE (HSE) conduction

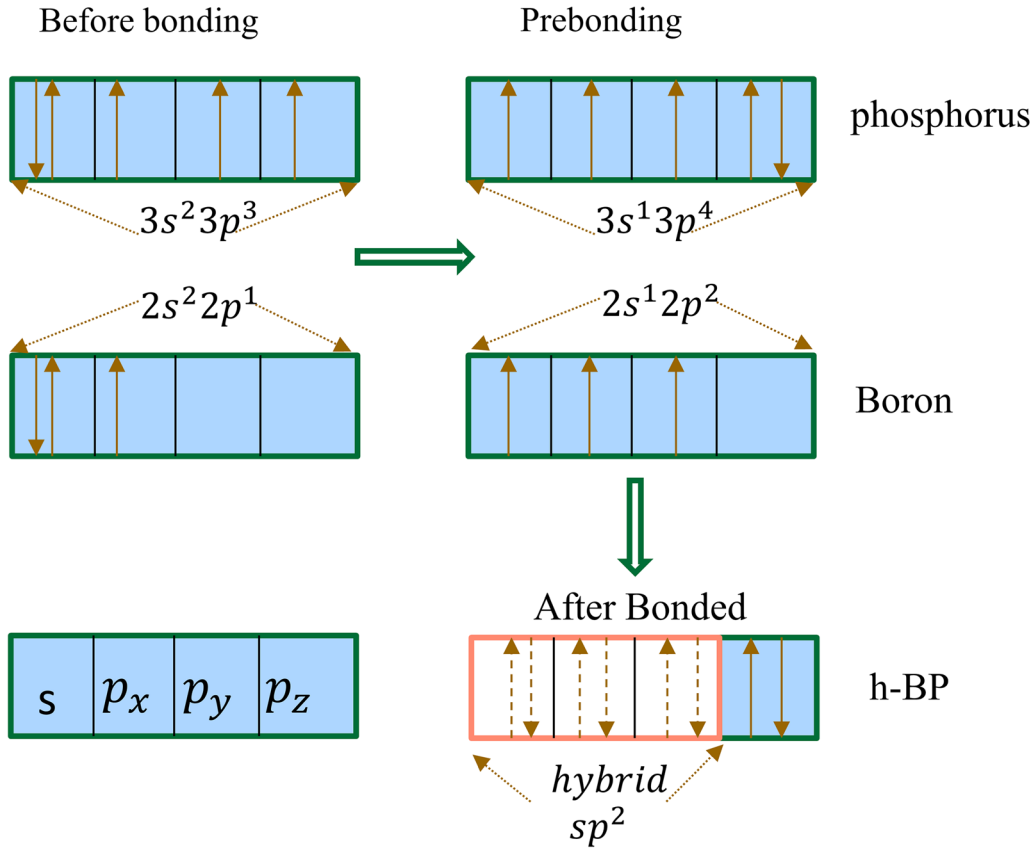


Fig. 3. The schematic of electron configuration in h-BP, phosphorus and boron are configured as  $3s^2 3p^3$  and  $2s^2 2p^1$  before bonding, respectively, and then are reconfigured as  $3s^1 3p^4$  and  $2s^1 2p^2$ , respectively, during the prebonding process, and finally is hybridized as  $sp^2$  to maintain the planar structure of h-BP.

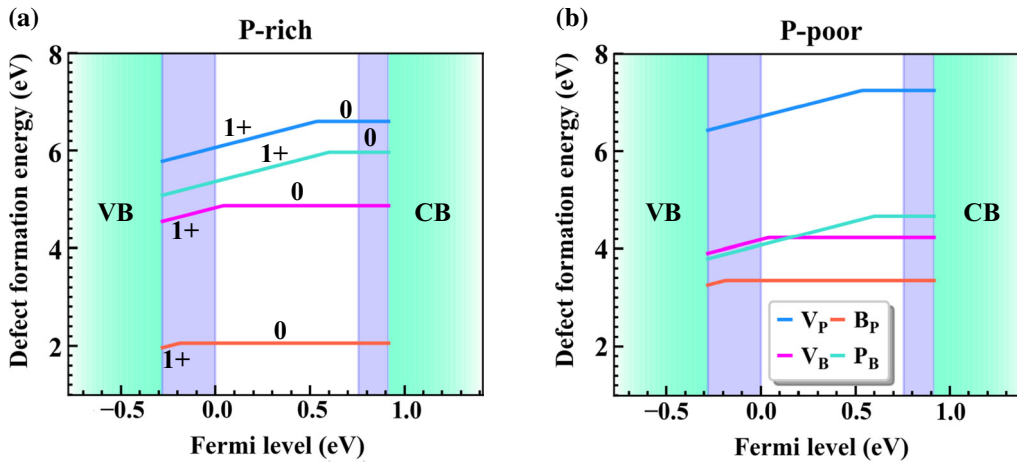


Fig. 4. Calculated formation energies of the native defects of  $V_B$ ,  $V_P$ ,  $P_B$ ,  $B_P$  in h-BP monolayer for their stable charge states as a function of the Fermi level in (a) phosphorus-poor and (b) phosphorus-rich limit conditions. The PBE (HSE) conduction band and valence band are labeled in blue (green). By referencing HSE VBM to zero point, the CTLs can be rescaled from PBE to HSE values (Color figure online).

band and valence band are labeled. By referencing HSE VBM as zero point, the CTLs can be rescaled from PBE to HSE values. As shown in Fig. 4, under both phosphorus-poor and -rich conditions,  $B_P$  is the most energy favorable defect for the h-BP monolayer but is a deep donor. That is, the CTL of  $E_{(1+/0)}$  (see next section) was found to be located close to

HSE VBM. In our previous paper,<sup>48</sup> we found that under N-poor conditions  $V_N$  ( $B_N$ ) is the most energy favorable defect in  $p(n)$ -doping h-BN, while under N-rich conditions, the most energy favorable defect becomes  $N_B$ . The discrepancy here can be explained by the different bond lengths and binding energy as shown in our previous work.<sup>19</sup> The  $V_B$  also seems to

be a deep donor with higher formation energy than  $B_P$ . As shown in Fig. 4, both  $B_P$  and  $V_B$  are found to be 1+ charge state near the VBM. Thus, one electron occupying the defect state tends to transfer to the valence bands and further recombines with a hole. Consequently, this means that  $B_P$  and  $V_B$  act as hole trap centers in the  $p$ -type doping h-BP monolayer and degrade the  $p$ -doping efficiency of the h-BP monolayer. Both  $V_P$  and  $V_B$  show a shallow donor under phosphorus-poor (P-poor) conditions. However, the formation energy of  $V_P$  is found much higher than that of  $P_B$ , indicating that the concentration of phosphorus vacancy in the h-BP monolayer is much lower under thermodynamic equilibrium. In contrast, under the phosphorus-rich (P-rich) condition,  $B_P$  is still the most stable defect in the whole range of electron chemistry potential. The results can be speculated from the atomic radius, that is, a smaller atom (boron) can more easily occupy the site belonging to a larger one (phosphorus) and it is harder in the opposite case. As a deep donor,  $B_P$  with a small formation energy seriously affects  $p$ -doping in the h-BP monolayer.  $V_P$  and  $P_B$  are shallow donors in the phosphorus-rich condition; however, the large value of formation energy for both defects indicate that the concentration can be ignored under thermodynamic equilibrium.

Based on Fig. 4, no negative-U character<sup>61</sup> is found; in other words, all the charge transition levels (CTLs, see “[Thermodynamic Transition](#)”) are determined by two continuous charge states. Thus, the result indicates that the unusually large lattice relaxations of the four types of defects not exist, meaning that our supercells (144 atoms) are large enough in this study. By comparing P-poor and P-rich conditions,  $B_P$  is found to be the most energy favorable defect in h-BP and acts as a hole trap center. Thus,  $p$ -type doping in the h-BP monolayer under the P-rich condition is not desired.

### Thermodynamic Transition

When the defects are spontaneously produced in the h-BP monolayer, different charge states appear. The CTL corresponding to transitions from one state of charge to another is determined by Eq. 3:

$$E_{(q/q')} = \frac{E^f(q; E_f = 0) - E^f(q'; E_f = 0)}{q - q'} \quad (3)$$

where  $E^f(q; E_f = 0)$  and  $E^f(q'; E_f = 0)$  represent the formation energies for the states of charge  $q$  and  $q'$ .<sup>62</sup> The energy difference between CTL and CBM/VBM determines the donor/acceptor ionization energy. Thus, CTL is an intuitive physical quantity to character nature (donor or acceptor) of a given defect. The CTLs can be intuitively obtained in Fig. 4. That is, different slopes represent different charge states, and the inflection point of the slope

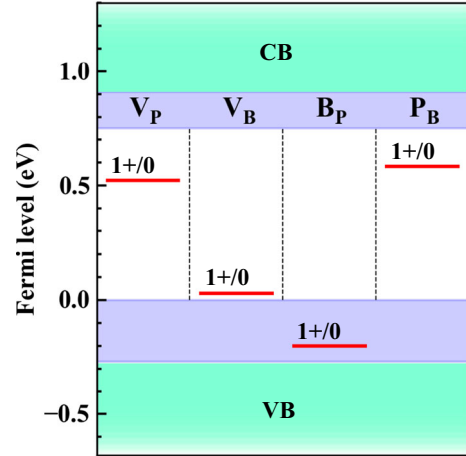


Fig. 5. Stable charge states and charge transition levels of the native defects of  $V_B$ ,  $V_P$ ,  $P_B$ , and  $B_P$  in the h-BP monolayer, the charge transition levels are labeled in red, and the PBE (HSE) conduction band and valence band are labeled in blue (green). The practical HSE CTLs are illustrated in the first column. By referencing HSE VBM to zero point, the CTLs can be rescaled from PBE to HSE values (Color figure online).

represents the CTLs. The CTLs calculated by the formula (3) are summarized in Fig. 5. It is clearly found that  $V_P$  and  $P_B$  are shallow donors while  $V_B$  and  $B_P$  are holes trap centers. The results indicate that during the  $p$ -doping process,  $V_B$  and  $B_P$  defects must be eliminated as much as possible, especially in the P-rich limitation where  $B_P$  is easily formed with a low defect formation energy.

### CONCLUSIONS

In this work, by using the first-principles method with state-of-the-art 2D defect corrected methods, we have systematically investigated the structural, electronic and magnetic properties of monolayer h-BP with charged defects, including  $V_P$ ,  $V_N$ ,  $P_B$  and  $B_P$ . The CTLs were calculated by considering various charged states. We found the MSCSs for all the four kinds of native defects are 0 and 1+ states. The results show that vacancy defects would induce defect levels in bandgap which are responsible for the total magnetic moment in the h-BP single layer. The charge transition levels of  $V_P$  and  $P_B$  are located close to the conduction band, indicating that they are shallow donors. However, neither of them will be produced with a considerable concentration under thermodynamic equilibrium conditions due to a high defect formation energy. In contrast, the charge transition levels of  $V_B$  and  $B_P$  are located near the valence band maximum, showing that they are deep donors. Specifically,  $B_P$  under the phosphorus-rich condition with a lower defect formation energy, acts as a hole trap center in the  $p$ -type doping h-BP monolayer, which seriously affects the efficiency of  $p$ -type doping and further constrains the  $p$ -type conductivity in BP-based novel devices.

## FUNDING

This research was funded by the National Natural Science Foundation of China, Grant Nos. 11664005 and 61564002; the Joint Foundation of Guizhou Normal University, Grant No. 7341; Scientific and Technological Cooperation Projects of Guizhou Province, China, Grant No. 2013-7019; Science and technology planning project of Guizhou province, Grant No. 2017-5736-009; Guizhou Science and Technology Foundation, Grant No. 20201Y021. Z. Gao acknowledges the financial support from MOE tier 1 funding of Singapore (Grant No. R-144-000-402-114).

## CONFLICT OF INTEREST

The authors declare no competing financial interests.

## REFERENCES

- P. Popper and T.A. Ingles, *Nature* 179, 1075 (1957).
- T.L. Chu, J.M. Jackson, A.E. Hyslop, and S.C. Chu, *J. Appl. Phys.* 42, 420 (1971).
- O.A. Golikova, *Phys. Status Solidi (a)* 51, 11 (1979).
- B. Stone and D. Hill, *Phys. Rev. Lett.* 4, 282 (1960).
- G. Li, J.K.C. Abbott, J.D. Brasfield, P. Liu, A. Dale, G. Duschler, P.D. Rack, and C.S. Feigerle, *Appl. Surf. Sci.* 327, 7 (2015).
- M. Feng, J. Zhang, H. Zhou, P. Jiang, D. Zhang, L. Wang, and S. Chen, *Mater. Res. Express* 6, 125922 (2020).
- H. Sugimoto, B. Somogyi, T. Nakamura, H. Zhou, Y. Ichihashi, S. Nishiyama, A. Gali, and M. Fujii, *J. Phys. Chem. C* 123, 23226 (2019).
- K.S. Novoselov, A.K. Geim, S.V. Morozov, D. Jiang, Y. Zhang, S.V. Dubonos, I.V. Grigorieva, and A.A. Firsov, *Science* 306, 666 (2004).
- K.S. Novoselov, A.K. Geim, S.V. Morozov, D. Jiang, M.I. Katsnelson, I.V. Grigorieva, S.V. Dubonos, and A.A. Firsov, *Nature* 438, 197 (2005).
- H. Liu, A.T. Neal, Z. Zhu, Z. Luo, X.F. Xu, D. Tomanek, and P.D. Ye, *ACS Appl. Nano Mater.* 8, 4033 (2014).
- Y.P.V. Subbaiah, K.J. Saji, and A. Tiwari, *Adv. Funct. Mater.* 26, 2046 (2016).
- J.H. Hong, C. Wang, H.J. Liu, X.B.A. Ren, J.L. Chen, G.Y. Wang, J.F. Jia, M.H. Xie, C.H. Jin, W. Ji, J. Yuan, and Z. Zhang, *Nano Lett.* 17, 6653 (2017).
- J.G. Feng, D. Biswas, A. Rajan, M.D. Watson, F. Mazzola, O.J. Clark, K. Underwood, I. Markovic, M. McLaren, A. Hunter, D.M. Burn, L.B. Duffy, S. Barua, G. Balakrishnan, F. Bertran, P. Le Fevre, T.K. Kim, G. van der Laan, T. Hesjedal, P. Wahl, and P.D.C. King, *Nano Lett.* 18, 4493 (2018).
- G. Kioseoglou, M. Korkusinski, T. Scrace, A.T. Hanbicki, M. Currie, B.T. Jonker, A. Petrou, and P. Hawrylak, *Phys. Status Solidi RRL* 10, 111 (2016).
- L.-B. Shi, Y.-Y. Zhang, X.-M. Xiu, and H.-K. Dong, *Carbon* 134, 103 (2018).
- H. Niu, X. Wang, C. Shao, Y. Liu, Z. Zhang, and Y. Guo, *J. Mater. Chem. A* 8, 6555 (2020).
- W.W. Luo, G. Liu, X. Wang, X.L. Lei, C.Y. Ouyang, and S.Q. Liu, *Phys. B* 537, 1 (2018).
- Z. Luo, Y. Yang, X. Yang, B. Lv, and X. Liu, *Mater. Res. Express* 6, 115915 (2019).
- X.-F. Liu, Z.-J. Luo, X. Zhou, J.-M. Wei, Y. Wang, X. Guo, B. Lv, and Z. Ding, *Chin. Phys. B* 28, 086105 (2019).
- Z.-F. Zhang, T.-G. Zhou, H.-Y. Zhao, and X.-L. Wei, *Chin. Phys. B* 23, 016801 (2014).
- Z. Zhang, Z. Geng, D. Cai, T. Pan, Y. Chen, L. Dong, and T. Zhou, *Phys. E* 65, 24 (2015).
- M. Chhowalla, D. Jena, and H. Zhang, *Nat. Rev. Mater.* 1, 16052 (2016).
- Y. Yin, C. Shao, C. Zhang, Z. Zhang, X. Zhang, J. Robertson, and Y. Guo, *ACS Appl. Mater. Interfaces* 12, 22378 (2020).
- Yu Tian-Tian, P.-F. Gao, Y. Zhang, and S.-L. Zhang, *Appl. Surf. Sci.* 486, 281 (2019).
- Y. Wang, C. Huang, D. Li, P. Li, Yu Jianguying, Y. Zhang, and X. Jinrong, *J. Phys. Condens. Matter* 31, 285501 (2019).
- M.M. Obeid, H.R. Jappor, K. Al-Marzoki, D.M. Hoat, T.V. Vu, S.J. Edrees, Z.M. Yaseen, and M.M. Shukur, *Comput. Phys. Commun.* 170, 109201 (2019).
- S. Ullah, P.A. Denis, and F. Sato, *Appl. Surf. Sci.* 471, 134 (2019).
- J. Wu, J.-H. Li, and Y.-X. Yu, *Phys. Chem. Chem. Phys.* 22, 7633 (2020).
- Z.Z. Zhou, H.J. Liu, D.D. Fan, G.H. Cao, and C.Y. Sheng, *Phys. Rev. B* 99, 085410 (2019).
- S. Ullah, P.A. Denis, and F. Sato, *ACS Omega* 3, 16416 (2018).
- D. Cakir, D. Kecik, H. Sahin, E. Durgun, and F.M. Peeters, *Phys. Chem. Chem. Phys.* 17, 13013 (2015).
- S. Wang and X. Wu, *Chin. J. Chem. Phys.* 28, 588 (2015).
- L. Shi, P. Li, W. Zhou, T. Wang, K. Chang, H. Zhang, T. Kako, G. Liu, and J. Ye, *Nanomater. Energy* 28, 158 (2016).
- H.R. Jiang, W. Shyy, M. Liu, L. Wei, M.C. Wu, and T.S. Zhao, *J. Mater. Chem. A* 5, 672 (2017).
- Y. Mogulkoc, M. Modarresi, A. Mogulkoc, and B. Alkan, *Phys. Chem. Chem. Phys.* 20, 12053 (2018).
- A. Mogulkoc, Y. Mogulkoc, M. Modarresi, and B. Alkan, *Phys. Chem. Chem. Phys.* 20, 28124 (2018).
- S. Ullah, P.A. Denis, M.G. Menezes, and F. Sato, *Appl. Surf. Sci.* 493, 308 (2019).
- B. Zeng, M. Li, X. Zhang, Y. Yi, L. Fu, and M. Long, *J. Phys. Chem. C* 120, 25037 (2016).
- B. Bhattacharya, J. Deb, and U. Sarkar, *AIP Adv.* 9, 095031 (2019).
- T. Malin, V. Mansurov, Y. Galitsyn, and K. Zhuravlev, *Phys. Status Solidi C* 12, 443 (2015).
- Z.Y. Al Balushi, K. Wang, R.K. Ghosh, R.A. Vila, S.M. Eichfeld, J.D. Caldwell, X. Qin, Y.C. Lin, P.A. DeSario, G. Stone, S. Subramanian, D.F. Paul, R.M. Wallace, S. Datta, J.M. Redwing, and J.A. Robinson, *Nat. Mater.* 15, 1166 (2016).
- Y. Chen, K. Liu, J. Liu, T. Lv, B. Wei, T. Zhang, M. Zeng, Z. Wang, and L. Fu, *J. Am. Chem. Soc.* 140, 16392 (2018).
- W. Wang, Y. Zheng, X. Li, Y. Li, H. Zhao, L. Huang, Z. Yang, X. Zhang, and G. Li, *Adv. Mater.* 31, 1803448 (2019).
- M.R.A. Monazam, U. Ludacka, H.-P. Komsa, and J. Kotakoski, *Appl. Phys. Lett.* 115, 0716041 (2019).
- C.G. Van de Walle and J. Neugebauer, *J. Appl. Phys.* 95, 3851 (2004).
- C. Freysoldt, B. Grabowski, T. Hickel, J. Neugebauer, G. Kresse, A. Janotti, and C.G. Van de Walle, *Rev. Mod. Phys.* 86, 253 (2014).
- A. Janotti and C.G. Van de Walle, *Phys. Rev. B* 76, 165202 (2007).
- X. Liu, Z. Gao, V. Wang, Z. Luo, B. Lv, Z. Ding, and Z. Zhang, *ACS Appl. Mater. Interfaces* 12, 17055 (2020).
- C. Freysoldt and J. Neugebauer, *Phys. Rev. B* 97, 2054251 (2018).
- D. Broberg, B. Medasani, N.E.R. Zimmermann, G. Yu, A. Canning, M. Haranczyk, M. Asta, and G. Hautier, *Comput. Phys. Commun.* 226, 165 (2018).
- G. Kresse and J. Furthmüller, *Phys. Rev. B* 54, 11169 (1996).
- J.P. Perdew, K. Burke, and M. Ernzerhof, *Phys. Rev. Lett.* 77, 3865 (1996).
- P.E. Blöchl, *Phys. Rev. B* 50, 17953 (1994).
- J. Heyd, G.E. Scuseria, and M. Ernzerhof, *J. Chem. Phys.* 124, 219906 (2006).
- V. Wang, N. Xu, J.-C. Liu, G. Tang, and W.-T. Geng, <https://arxiv.org/abs/1908.08269>. Accessed on 25 August 2019 (2019).
- M.H. Naik and M. Jain, *Comput. Phys. Commun.* 226, 114 (2018).

57. T.A. Manz, *J. RSC Adv.* 7, 45552 (2017).
58. T.A. Manz and N.G. Limas, *RSC Adv.* 6, 47771 (2016).
59. N.G. Limas and T.A. Manz, *RSC Adv.* 6, 45727 (2016).
60. N. Berseneva, A.V. Krasheninnikov, and R.M. Nieminen, *Phys. Rev. Lett.* 107, 0355011 (2011).
61. P. Li, S. Deng, L. Zhang, G. Liu, and J. Yu, *Chem. Phys. Lett.* 531, 75 (2012).
62. R. González, W. López-Pérez, Á. González-García, M.G. Moreno-Armenta, and R. González-Hernández, *Appl. Surf. Sci.* 433, 1049 (2018).

**Publisher's Note** Springer Nature remains neutral with regard to jurisdictional claims in published maps and institutional affiliations.